C. R. Mecanique 341 (2013) 4–14

Contents lists available at SciVerse ScienceDirect

Comptes Rendus Mecanique

www.sciencedirect.com

Combustion, flow and spray dynamics for aerospace propulsion

Characterization of the coherent structures in swirling flames stabilized in a two-staged multi-injection burner: Influence of the staging factor

Caractérisation des structures cohérentes dans des flammes swirlées dans un injecteur multipoint étagé: Influence de l'étagement

Theodore Providakis [a,b,*], Laurent Zimmer [a,b], Philippe Scouflaire [a,b], Sébastien Ducruix [a,b]

[a] *CNRS, UPR 288, Laboratoire EM2C, 92290 Châtenay-Malabry, France*
[b] *École Centrale Paris, 92290 Châtenay-Malabry, France*

ARTICLE INFO

Article history:
Available online 9 January 2013

Keywords:
Combustion
Swirling flame
Staging factor

Mots-clés :
Combustion
Flamme swirlée
Étagement

ABSTRACT

Staged multi-injection combustors seem good candidates to face flame stabilization problems (combustion instabilities, flashback, flame extinction), encountered in lean premixed prevaporized (LPP) burners. Staging procedures enable fuel distribution control while multipoint injection can lead to a fast and efficient mixing. In the present study, a laboratory-scale staged multipoint combustor is characterized using High Speed Particle Image Velocimetry and Planar Laser Induced Fluorescence measurements. It is shown that the fuel distribution strongly affects the flame stabilization processes, modifying the thermo-acoustic coupling. Furthermore, results reveal the presence of a precessing vortex core (PVC), that can lead to a better flame stabilization in particular cases.

RÉSUMÉ

Les injecteurs multipoints étagés semblent de bons candidats pour faire face aux problèmes de stabilité de flamme (instabilités de combustion, flashback, extinction de flamme) rencontrés dans les brûleurs à combustion prémélangée prévaporisée pauvre. Les procédures d'étagement permettent de contrôler la distribution de carburant tandis que l'injection multipoint peut conduire à un mélange plus rapide et plus efficace. Dans cette étude un injecteur multipoint étagé à échelle de laboratoire est caractérisé à l'aide de la Vélocimétrie par Image de Particules à haute cadence et la Fluorescence Induite par Laser. Les résultats montrent que les processus de stabilisation de flamme sont fortement influencés par la distribution de carburant, conduisant à des instabilités thermo-acoustiques plus ou moins élevées. Par ailleurs, les résultats révèlent la présence d'une structure aerodynamique en précession, qui, sous certaines conditions, améliore la stabilisation de la flamme.

* Corresponding author at: CNRS, UPR 288, Laboratoire EM2C, 92290 Châtenay-Malabry, France.
E-mail addresses: theodore.providakis@ecp.fr (T. Providakis), laurent.zimmer@ecp.fr (L. Zimmer), philippe.scouflaire@ecp.fr (P. Scouflaire), sebastien.ducruix@ecp.fr (S. Ducruix).

1631-0721/$ – see front matter
http://dx.doi.org/10.1016/j.crme.2012.10.010

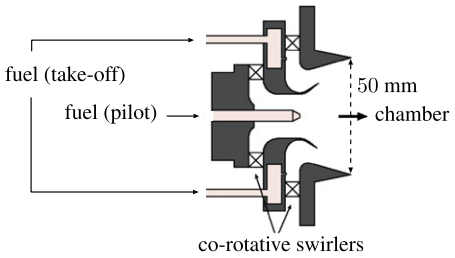

Fig. 1. Schematic view of the injection device. Flow from left to right.

1. Introduction

Due to environmental concerns, permissible pollutant emissions of gas turbine plant or aircraft engines have been significantly decreased in recent years [1]. Combustion in gas turbines was traditionally based on non-premixed flames for various reasons (safety, stability), but this type of combustion usually leads to large pollutant emissions (NO_x, CO, ...). To face this issue, Lean Premixed Prevaporized (LPP) regimes are envisaged in new generation combustors [2–4]. This concept consists in providing a uniform lean mixture of fuel and air that burns at lower temperature, mainly reducing thermal NO_x emissions. Unfortunately gas turbines operating in lean conditions often present high combustion dynamics, leading to stability issues such as combustion instabilities, flashback, self-ignition and blowout [5]. In particular, the coupling of heat release and pressure oscillations in the combustor can produce self-excited oscillations of such an amplitude that they may damage the combustor [6–8]. It is known that these acoustic interactions tend to develop more easily in partially and perfectly premixed combustion systems such as the LPP ones [9]. As an example of what can be envisaged to overcome those problems, secondary fuel injection has been proposed, for which a small amount of fuel is injected upstream to constitute a pilot flame region. This secondary injection can also be modulated so as to reduce coupling between heat release and pressure while keeping reduced emission levels [10–14].

Multi-injection staged injectors are now considered as potential candidates for real engine operation. Staging procedures can add a supplementary degree of freedom in terms of fuel distribution, while multipoint injections can lead to a fast and efficient mixing. However, the dynamics of these new generation injection devices must still be studied to clearly determine their stability properties and to optimize spatial fuel distribution.

The present article concerns the study of a multi-injection system, fed with liquid fuel (dodecane) to be more representative of practical applications. Operating with a liquid fuel adds new critical parameters such as droplet distribution and evaporation, that strongly influence the dynamics of the flame. Depending on the type of atomizer used for fuel injection, strong fluctuations can be encountered in the resulting spray [15]. In the present study, a laboratory-scale staged multipoint combustor is developed in the framework of LPP combustion. Depending on the regime and staging factor, strong combustion instabilities can be encountered. Using the staging procedure between the primary and the secondary stages as defined in [16], droplet and velocity field distributions can be varied in the spray that is formed at the entrance of the combustion chamber. Three staging values, corresponding to three different flame stabilization processes, are analyzed, while power is kept constant. The reactive flow is characterized using High Speed Particle Image Velocimetry and Planar Laser Induced Fluorescence. Spray and flame dynamics are analyzed using spectral post-processing. A synchronized phase-lock averaging procedure is finally proposed to go deeper in the understanding of the highly coupled dynamics.

2. Experimental setup

The injection system is composed of two stages where air and liquid fuel flow and mix. The resulting mixture enters a rectangular combustion chamber ($500 \times 150 \times 150$ mm), composed of two silica windows for optical access and two water-cooled walls.

2.1. Injection device

A schematic view of the injection device is shown in Fig. 1. Inside this device, the upstream (primary) stage is called 'pilot stage'. It is composed of a pressurized nozzle for fuel distribution and a swirler for air injection. The pressurized nozzle generates a solid cone and fuel can be injected at a maximum flow rate of 6.3 liters per hour. Its flow number is equal to 1.4 $\mathrm{l\,h^{-1}\,bar^{-0.5}}$. The air swirler is composed of 18 vanes and it is geometrically designed so that 20% of the global air rate flows through this stage. This has been experimentally verified and details can be found in [17]. The downstream (secondary) stage is called the 'Take-off stage'. It is composed of a multipoint system for fuel and a swirler for air. The multi-injection system is composed of 10 equally-spaced holes (0.3 mm in diameter). The swirler is composed of 20 vanes and it has been designed so that 80% of the global air rate flow through this stage. Both swirlers are set co-rotating (but this

Table 1
Operating and pressure conditions. $Pw = 85$ kW, $\phi = 0.6$, $P_a = 101\,325$ Pa. ΔP_a is the pressure drop through the injection device.

Condition	$\dot{m}_a$ [g s^{-1}]	$\dot{Q}_{f,g}$ [l h^{-1}]	α [%]	$\Delta P_{f,t}$ [bar]	$\Delta P_{f,p}$ [bar]	$\Delta P_a/P_a$ [%]
OP_{20}	50	9.4	**20**	0.13	1.9	15
OP^{+}_{60}	50	9.4	**60**$^{+}$	0.08	18	15
OP^{-}_{60}	50	9.4	**60**$^{-}$	0.08	18	15

could easily be modified) and designed so that the theoretical swirl number S based on geometrical considerations is close to 1 [18]. To enhance fuel vaporization, air is preheated at 473 K.

2.2. Operating conditions

As staging is one of the main features of this type of injection system, a staging factor α is defined to quantify the relative amount of fuel injected through the primary (pilot) stage [16]:

$$\alpha = \frac{\dot{m}_{f,p}}{\dot{m}_{f,g}} \times 100 \tag{1}$$

where $\dot{m}_{f,g}$ is the total fuel flow rate and $\dot{m}_{f,p}$ is the fuel flow rate through the primary stage. As a consequence, α will be zero in case all fuel flows through the secondary (take-off) stage and 100% when all the fuel is injected through the pilot stage.

Table 1 shows the operating conditions chosen for the present study. The global air and fuel flow rates are kept constant (constant power and global equivalence ratio) while α is varied from 20 to 60%, a domain where the shape of the flame is highly influenced by the stage procedure. Moreover, for a given staging value, two types of flames can be encountered, whether α is increased from 20 to 60% or decreased from 60 to 20%. This is related to a hysteresis phenomenon and subsequently, we must define α^{+} and α^{-}, corresponding to increasing or decreasing staging values.

For values of α^{-} higher than 40% (pilot stage regimes), the flame stabilization process is controlled by the pilot stage, leading to a compact V-flame, anchored inside the injection device. For values of α^{-} lower than 25% (take-off stage regimes), the flame is stabilized thanks to the take-off stage and takes an M-shape. In-between, there seems to be a competition between both stages, leading to a tulip-like shape of the flame. This later case will not be discussed in the present study, where measurements focus on two values of the staging factor (20 and 60%), representative of the two main flame shapes. Finally, for all values of α^{+}, the flame presents an M-shape similar to the one observed for values of α^{-} lower than 25%. Thermo-acoustic and aerodynamic activities are visible in both cases, probably associated with a more or less strong acoustic/aerodynamic coupling depending on the fuel staging.

2.3. Diagnostics

2.3.1. Spray characterization

The spray is characterized using High Speed Particle Image Velocimetry (HSPIV) in the axial direction. It was decided to use fuel droplets as particle tracers (no seeding). The camera collects the Mie scattering signal from individual droplets traversing the laser sheet. It is assumed that, at the exit of the injection system, most of the droplets are small enough to describe the aerodynamic flow. The laser sheet is generated by a system consisting of two Nd:YAG lasers (*Quantronix*). Both lasers emit pulses at a wavelength of 532 nm with an energy of 5 mJ per pulse and a temporal width of 120 ns at 20 kHz. An optical system (*Melles Griot*) is used to convert the laser beam into a planar light sheet 100 mm wide and 1 mm thick. Both sides of the combustion chamber include large rectangular silica windows. For the axial measurements, two small rectangular quartz windows (100 mm long and 15 mm wide) were designed and placed in the upper and lower walls of the combustion chamber, allowing the laser sheet to cross the chamber in the axial direction on its centerline.

A fast speed camera (Photron Fastcam SA5, 1024×1024 pixels at 6000 frames per second) equipped with a 105 mm $F/2.8$ Nikon Nikkor objective is used to acquire the resulting images. The two lasers work at half the camera's acquisition frequency, f_{cam}, and are synchronized by a pulse delay generator (BNC 555 pulse/delay Generator). The time delay, δt, between two pulses has been chosen so that the displacement of a droplet does not exceed one fourth of the processing window size, which is 16×16 pixels in this study. The acquisition parameters are summarized in Table 2 and a schematic view of the setup is presented in Fig. 2(b).

2.3.2. Mie fluctuations

In addition to the Mie scattering signal acquired during the HSPIV campaign, an He–Ne laser beam ($\lambda = 632$ nm) is positioned so as to pass through the spray, in its lower region where the density of droplets is high and at 4 mm from

Table 2
PIV acquisition parameters.

	f_{cam} [kHz]	δt [μs]	Nb of raw images [–]	Image size [px]	Camera pitch [mm/px]	Sheet position [mm]
Axial	20	6	12 000	776 × 448	0.15	$y = 0$ central axis

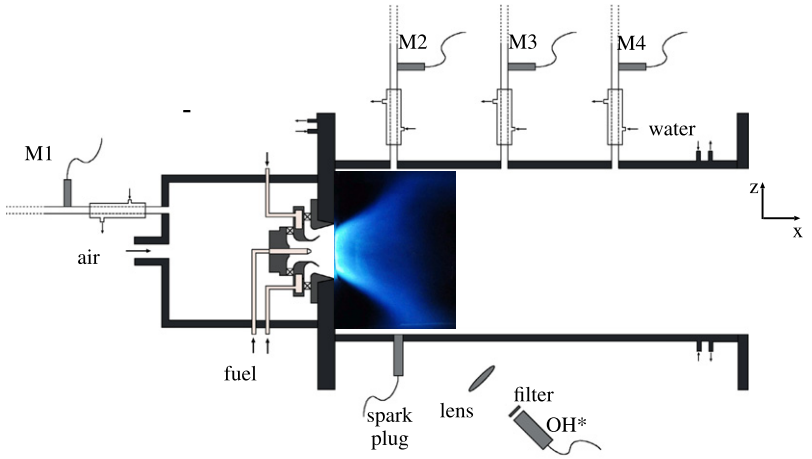

(a) Pressure and heat release measurement setup (OP^{-}_{60} flame image)

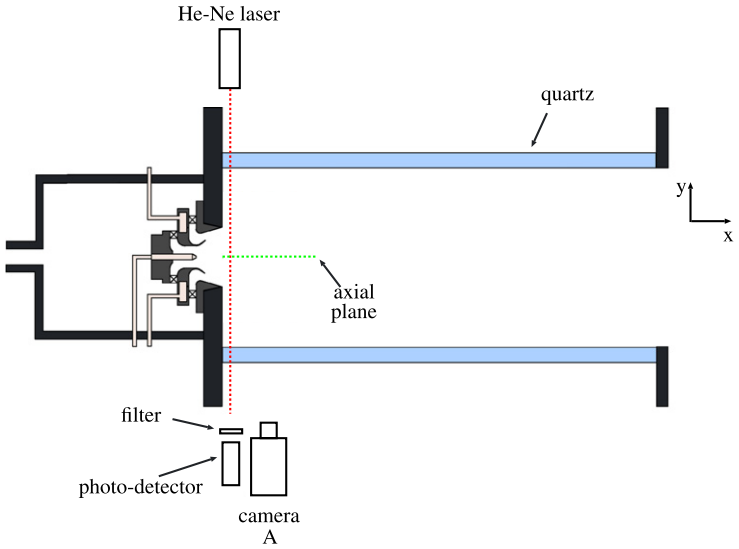

(b) Laser diagnostics setup.

Fig. 2. Experimental setups.

the injection exit. A photo-detector, coupled with a filter ($\lambda = 632 \pm 10$ nm), is used to collect intensity fluctuations. It is assumed that the fluctuations of the collected signal are proportional to the Mie fluctuations of the spray. A variation of the Mie signal is the result of a variation in droplet size or droplet density (resulting in a opposite variation of the transmitted light through the spray). As will be seen in the following, the use of this signal improves the dynamic analysis of the droplet's behavior.

2.3.3. Flame structure characterization

The reaction zone is characterized using Planar Laser Induced Fluorescence (PLIF) measurements in axial planes. The PLIF technique is carried out by exciting the OH radical, which is a good tracer to describe the structure of the flame. The laser

Table 3
OH-PLIF acquisition parameters.

	f_{cam} [Hz]	Exposure time [ns]	Nb of raw images [–]	Image size [px]	Camera pitch [mm/px]	Sheet position [mm]
Axial	10	100	10 000	512×512	0.15	$y = 0$ central axis

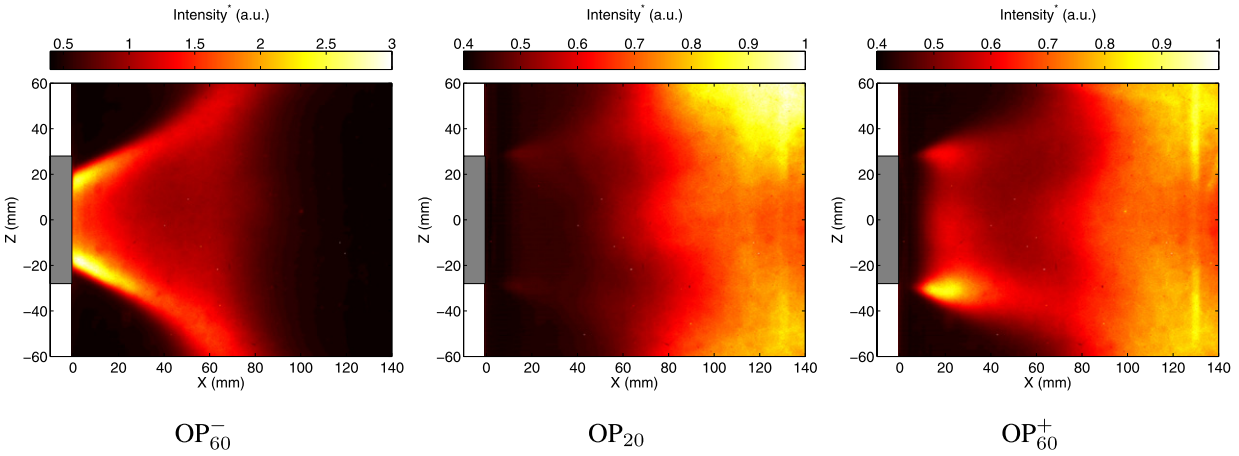

Fig. 3. Average OH* chemiluminescence for the three operating points. The intensity scale is normalized by the maximum value of OP_{20}.

sheet is generated by a system consisting of an Nd:YAG laser (*Continuum Powerlite DLS 8010 series*), emitting a pulse at a wavelength of 532 nm, coupled to a Dye Laser (*Continuum ND6000*). The Dye laser possesses a UV Tracker that doubles the laser output to cover the 206 nm and 425 nm wavelength ranges. A cylindrical diverging and a spherical converging lenses with respective focal lengths at 250 mm and 300 mm are used to generate a laser sheet 70 mm wide and 1 mm thick. The OH radical can be excited at different wavelengths but the emitted intensity changes. For this study, the maximum intensity was detected for a wavelength, λ, of 282.904 nm.

Images are acquired through an Intensified CCD camera (Princeton Instruments PI-MAP 3, 1024×1024 pixels at a rate of 15 images per second) equipped with a 105 mm $F/4.5$ Nikon Nikkor UV objective coupled to two interferential filters (*Melles Griot*, WG 305 and UG 11) centered on the OH radical emission band. Measurements are carried out at 10 Hz and the acquisition parameters are summarized in Table 3.

2.3.4. Pressure and heat release fluctuations

Four Bruel and Kjaer microphones (M1 to M4) are placed in semi-infinite water cooled waveguides that are flush-mounted close to the injection device and on the combustion chamber axis to measure pressure fluctuations (Fig. 2(a)). A photomultiplier (*Hamamatsu*, H5784-04), coupled with a filter ($\lambda = 310 \pm 10$ nm) and a spherical lens (focal = 300 mm) to collect all the light emitted by the flame, is used to measure OH* intensity fluctuations. This last signal is supposed to be proportional to the heat release rate for premixed flames [19], giving access to heat release fluctuations, a crucial quantity in the understanding of combustion instabilities. In the case of partially premixed flames, several studies [20,21] have shown that the OH* emission still provides qualitative information on the heat release fluctuations, on a global point of view.

All signals are acquired simultaneously on a multi-port acquisition card (*National Instruments*), at a rate of 16 kHz during 4 seconds for the HSPIV measurements and 60 seconds for the OH-PLIF ones.

3. Results and discussion

3.1. Flame stabilization

Fig. 3 shows the average OH* chemiluminescence for the three operating points. When operating at high staging factor (decreasing the staging factor to get to the operating point OP_{60}^{-}), the flame stabilization process is mainly controlled by the pilot stage resulting in a V-flame shape. This shape is observed for staging values higher than 40%. For lower staging factors, the amount of fuel delivered through the pilot stage becomes insufficient to keep the flame stabilized close to the pilot stage, resulting on a M-shape flame completely stabilized in the combustion chamber. In this case, the flame is mainly controlled by the take-off stage and the flame is anchored at the exit of the injection system (OP_{20}). From the OH* averaged fields, it seems that the major combustion process takes place far downstream in the combustion chamber but a small reaction rate is still visible close to the injection device. When the fuel is no longer injected through the pilot stage

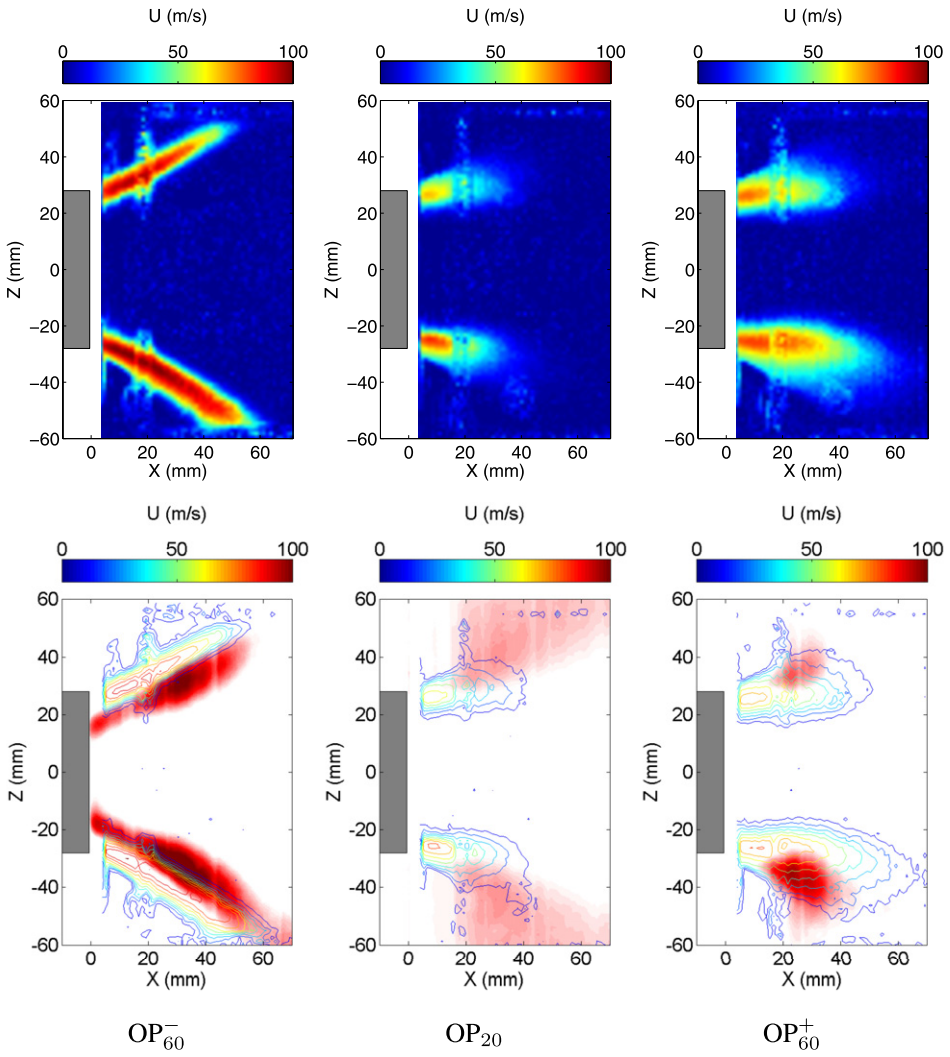

Fig. 4. Average droplet velocity magnitude (up) and OH-PLIF (bottom) fields for the three operating points. Contour lines of the velocity magnitude have been added to OH-PLIF fields. The intensity scale of the OH-PLIF fields is normalized by the maximum value of OP_{20}.

($\alpha = 0\%$), the flame becomes very unstable and is quickly extinguished. Finally, increasing the staging factor, while the flame is stabilized in the combustion chamber and before extinction ($OP_{20} \rightarrow OP_{60}^{+}$), results in a shape close to the OP_{20} one. This is the result of a hysteresis phenomenon and the flame does not return to its initial shape OP_{60}^{-}. Although both OP_{20} and OP_{60}^{-} present similar flame shapes, the combustion process is highly modified. Indeed the latter case shows a larger and more intense reaction region close to the injection device, enhancing the anchoring of the flame at the exit of the burner and improving its stability.

3.2. Velocity fields

Fig. 4 shows the average droplet velocity magnitude and OH-PLIF axial fields for the three operating points. The intensity scale of OH-PLIF fields is normalized by the maximum value of OP_{20}. The velocity field provides a quantitive information on the droplet's velocity but also a qualitative information on the spray's shape. For the OP_{60}^{-} case, the spray has a wide angle while for the OP_{20} and OP_{60}^{+} the angle of the spray is lower. Also, in these latter cases, the length of the spray is lower than in the OP_{60}^{-} case. This is the result of the flame's behavior as it has been shown in [22] that the spray's shape in non reactive conditions is not affected by the fuel distribution. It has also been found in [23] that OP_{20} generates lower size droplets at the exit of the injection device, thus resulting in a shorter spray.

The OP_{60}^{-} case presents faster droplets with velocities up to 100 $m\,s^{-1}$ in the center region of the spray, corresponding also to the region where droplets of lower size are found. Although the OP_{60}^{+} case presents the same fuel distribution, lower

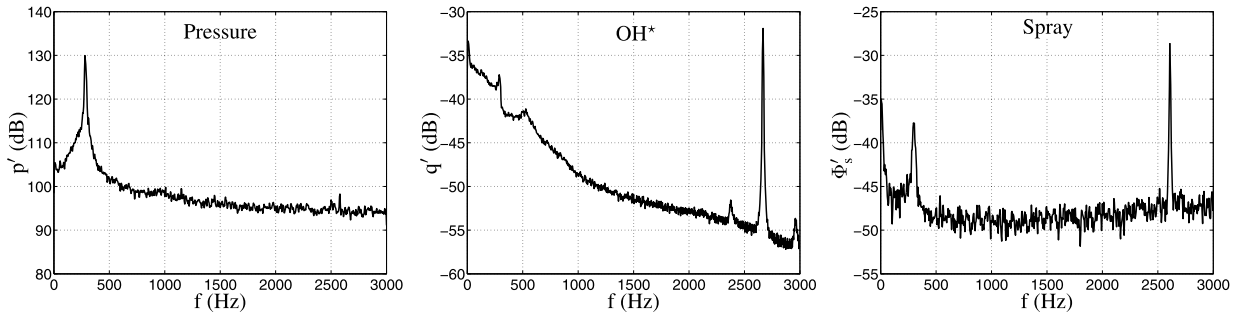

a) Pressure b) Heat release c) Surface flux

Fig. 5. PSD of the acoustic pressure (from microphone M2), heat release rate (OH* chemiluminescence) and spray's surface flux for the OP_{60}^{-} case.

velocities are achieved (up to 80 $m\,s^{-1}$). This is a direct consequence of the two different flame shapes. In one case, the flame is well stabilized in the pilot region inside the injection device and in the other one, it is anchored at the exit of the injection system. This results in a smaller area restriction due to the dilatation process in the injection region, thus inducing lower velocities for both OP_{20} and OP_{60}^{+}.

3.3. Combustion process

Analyzing the OH-PLIF average fields coupled to the PIV ones (Fig. 4), it is found that the interaction between droplets and flame is highly influenced by the staging factor and flame position. For the OP_{60}^{-} case, the majority of the spray surrounds the flame and the reaction process occurs in the inner region of the spray. Meanwhile, as mentioned earlier, for the OP_{20} case, the main reaction process takes place far downstream in the combustion chamber even though smaller droplets were measured in this case [23]. However, the PIV fields show that the generated spray is much larger in comparison to the OP_{60}^{-} case. Since the flame is farther downstream, temperatures close to the injection device are lower and droplets take more time to evaporate. When increasing the staging factor, while keeping the flame in the combustion chamber, a more intense reaction zone takes place near the injection device (OP_{60}^{+}). This can be explained by two different processes: (1) it was verified that augmenting the fuel flowrate through the pressurized nozzle results in a decrease of the size of the generated droplets. Therefore, a faster evaporation time will be achieved and the reaction process will happen sooner; (2) decreasing the amount of fuel through the takeoff stage enhances the atomization of the liquid jets and decreases the size of the droplets at the exit of the injection system [24]. Both effects may contribute to a faster reaction close to the injection system.

4. Unsteady flame dynamics

In addition to the pressure and OH* spontaneous emission signals, a He–Ne laser was used to acquire the fluctuations of the spray surface flux, as mentioned earlier. The laser is placed close to the injection exit so as to pass through a region of the spray, where most of droplets are found. Its position remains constant while changing the staging factor. Even though the properties change with the flame behavior, the acquired signal gives a qualitative information on the droplet's response to acoustic or aerodynamic instabilities. Furthermore, a spectral analysis can be applied to the HSPIV velocity fields to provide a quantitive information on velocity fluctuations. For each signal, a PSD is computed using the Welch method, with a spectral resolution of 4 Hz. Fig. 5 successively shows the PSD of the heat release rate (OH* chemiluminescence), acoustic pressure (from microphone M2), and spray's surface flux for the OP_{60}^{-} case.

The acoustic pressure reveals a strong peak centered at $f_{ac} = 300$ Hz, which is also seen by the OH* spontaneous emission, both in phase as expected by the Rayleigh criterion in the case of thermo-acoustic instabilities. As expected, the spray's surface flux fluctuations also shows a strong activity at the same frequency f_{ac}, revealing that this instability strongly modifies the spray's dynamics. More interestingly, a second peak centered at $f_{PVC} \approx 2600$ Hz with higher amplitude appears in the signal of heat release and flux surface fluctuations. It has been shown that this frequency corresponds to the presence of a precessing vortex core (PVC) in both non-reactive and reactive conditions [22,23]. Measurements in both conditions have shown that the PVC intensity is amplified with the presence of the flame, with an increase of the detected frequency due to higher flow temperatures, hence velocities. Finally, the OH* emission reveals two additional peaks with very low amplitudes around the peak of the PVC frequency, at $f \approx 2300$ Hz and $f \approx 2900$ Hz (Fig. 5(b)). This phenomenon has already been observed in [25,26] and recently analyzed in [27], where it is shown that these peaks correspond to a coupling phenomenon between the acoustics and the PVC. The detected frequencies correspond exactly to the sum and the difference of the acoustic and PVC ones ($f_{PVC} - f_{ac}$; $f_{PVC} + f_{ac}$). However, since the amplitude of these peaks is very low, no analysis is performed in the present study.

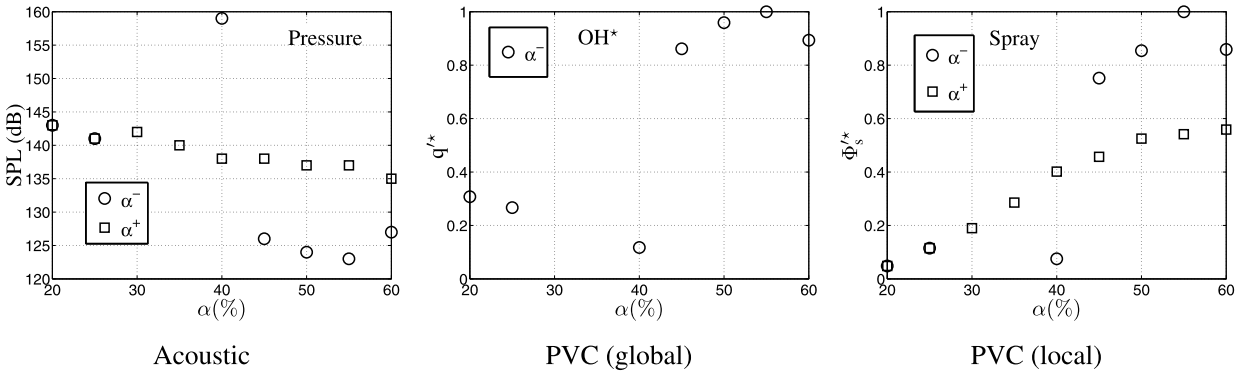

Fig. 6. Evolution of the PSD amplitude for the acoustic instability (left) and the PVC (middle and right) as a function of the staging factor. In the PVC analysis, intensities have been normalized by the maximum one achieved for $\alpha^- = 55\%$. No results are presented for the global PVC amplitude for α^+ values due to the low intensity of the light emitted by the flame at these operating conditions.

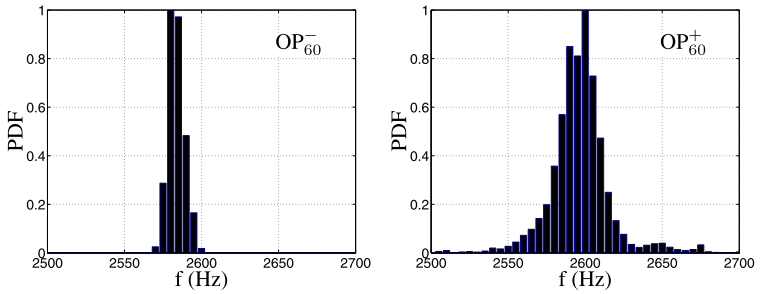

Fig. 7. PDF of the PVC frequency for $\alpha = 60\%$ and for two operating protocols OP^-_{60} and OP^+_{60}.

Fig. 6 shows the evolution of the PSD amplitude of the acoustic and PVC fluctuations as a function of the staging factor. For the acoustic fluctuations, the Sound Pressure Level (SPL) was computed by comparing the signal of a microphone M2 for all staging factors (α^- and α^+), while for the PVC, both surface flux and OH* signals were taken. However, when it comes to the flux surface signal, one must be careful with the obtained results. Indeed, the staging factor has a strong influence on the flame's shape and behavior, affecting the spray's dynamics as well. Therefore, surface flux fluctuations may also be related to a change in droplet diameter or density. Nevertheless, it is interesting to compare the evolution of the PVC as a function of the staging value through a global signal (OH*) and through a local one (surface flux).

When decreasing the staging factor, a strong acoustic instability is detected for $\alpha^- = 40\%$ and values lower than 30%. The first instability is the result of a transition phenomenon when the flame can no longer be stabilized in the pilot stage. This intense transition regime appears until $\alpha^- = 30\%$, making measurements barely possible. Then the flame stabilizes in the combustion chamber. When increasing back the staging factor, the flame remains stabilized in the combustion chamber with a small decrease of the acoustic amplitude until $\alpha^+ = 60\%$. Globally, results show that the V-flame, which is found for α^- between 40% and 60%, has a better stability than any other flame shape.

Concerning the PVC, both heat release and surface flux fluctuations present the same behavior, with a maximum amplitude value at $\alpha^- = 55\%$. Furthermore, at this operating point, the acoustic amplitude is found to be minimal. More broadly, results indicate an opposite behavior of the PVC amplitude and the acoustic one. This result has already been found in [27,28], where it is shown that the PVC can be suppressed by increasing the acoustic perturbation. This can be explained by the fact that the acoustic instability is mainly a motion in the axial direction while the PVC is in the azimuthal one.

By comparing the results obtained for $\alpha^- = 60\%$ and $\alpha^+ = 60\%$, where the same fuel distribution is injected, two distinct behaviors are found, OP^+_{60} revealing a strong acoustic activity while OP^-_{60} showing a strong aerodynamic instability. Because these two operating points present the same fuel staging but different fuel distributions, the following analysis will focus only on these two cases.

In order to understand the decrease in the PVC amplitude for the OP^+_{60} case, a wavelet transform analysis is performed in the spray's surface flux signal. The wavelet analysis can provide additional information on the temporal evolution of the PVC frequency. In this study, the chosen mother wavelet, $\psi(x)$, is the complex Morlet wavelet and it is defined as:

$$\psi(x) = \frac{1}{\sqrt{\pi f_b}} e^{2i\pi f_c x} e^{\frac{x^2}{f_b}} \tag{2}$$

where f_b is the bandwidth parameter and f_c is the wavelet center frequency. In the present study, these parameters are respectively equal to 50 and 7 Hz.

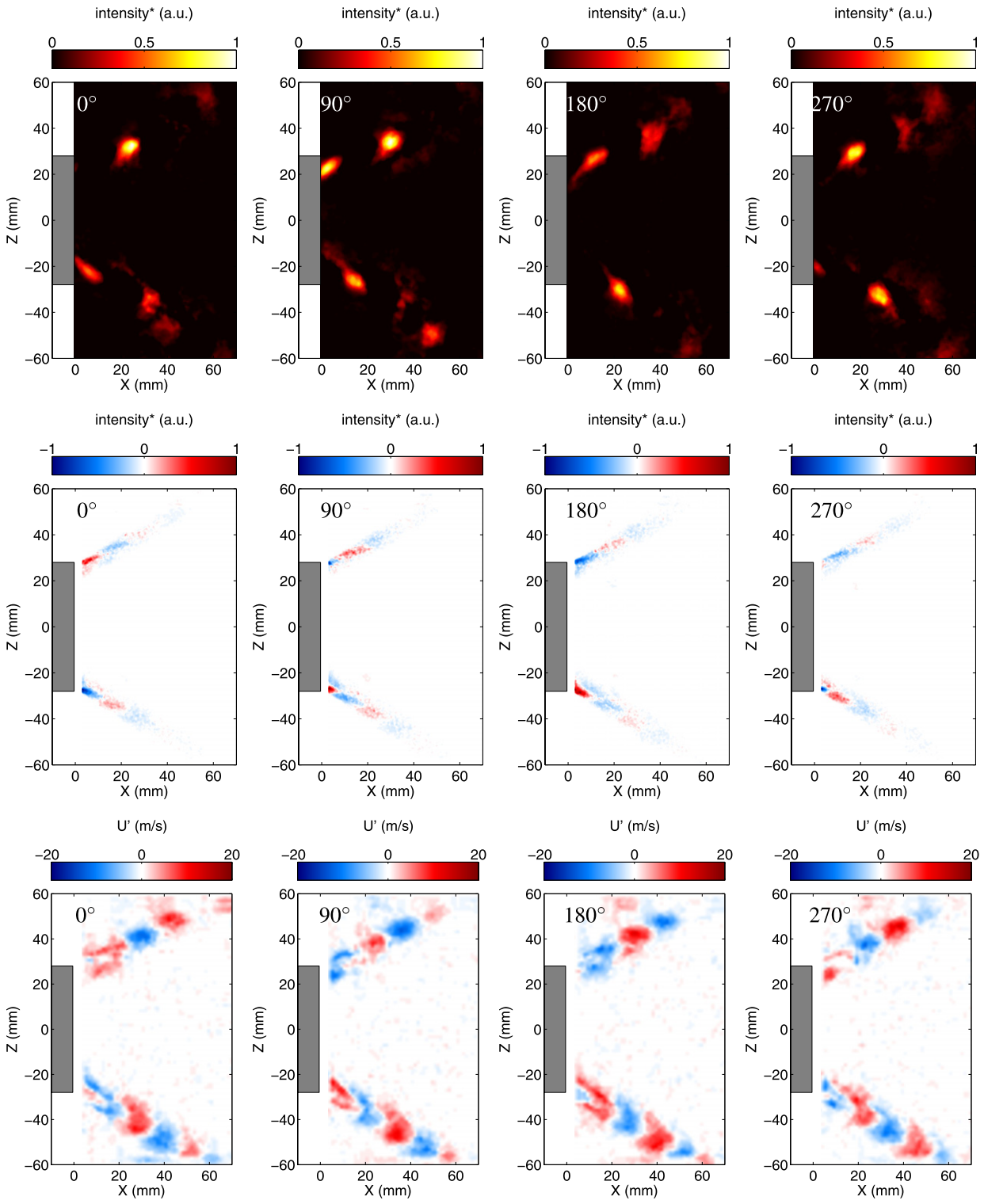

Fig. 8. Fluctuations of the phase averaged OH* emissions (top), Mie scattering intensity (middle) and droplet velocity magnitude (bottom), for four phases of the PVC cycle. OP_{60}^{-}, $f_{PVC} = 2580$ Hz.

Fig. 7 shows the PDF of the PVC frequency for OP_{60}^{+} and OP_{60}^{-} cases. Results reveal that for the V-flame (OP_{60}^{-}), where the acoustic instability is lower, the PVC frequency is mainly found at 2580 Hz with little fluctuations. When the flame is stabilized in the combustion chamber (OP_{60}^{+}), the resulting PDF has a Gaussian shape, centered at 2600 Hz, indicating that

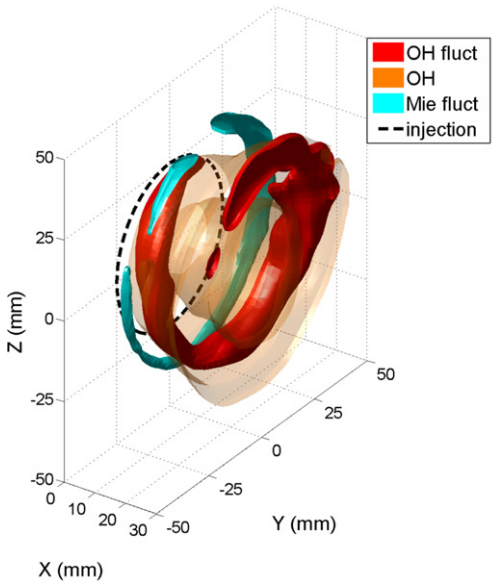

Fig. 9. Three-dimensional reconstruction of the PVC for the OP_{60}^{-} flame. The average OH emission is represented in orange giving the mean shape of the flame. OH and Mie fluctuations are respectively represented in red and blue.

the PVC frequency is strongly influenced by the higher acoustic perturbation level. The fact that the flame remains in the chamber for the same fuel distribution, may be explained by the unstable PVC and the high acoustic amplitude. Even if the interaction between acoustics and aerodynamics requires further investigations, it is likely that the flame stability and behavior are strongly influenced by the acoustic motion.

Lastly, the droplet's response to the PVC is analyzed by performing the phase-lock averaging method, focusing only on the OP_{60}^{-} case. Indeed, recent work on this subject [26] shows that, when two instabilities are strongly dependent (OP_{60}^{+} case), it is not possible to use this method to describe the flow behavior at one given frequency, neglecting the second one. In addition, this processing method can only be performed if the droplets are small enough to be considered as following the aerodynamic flow. Therefore, an estimation of the Stokes number (with respect to the PVC instability) has been computed and it was found that this number is much lower than 1 for a droplet size equal to 15 µm. Since the PDF of the droplets size distribution reported in [23] reveals that the generated spray is composed mainly of droplets below 15 µm, one expects them to follow the aerodynamic flow. Phase-lock averaging is computed at the frequency of the PVC, $f_{PVC} = 2580$ Hz, on the axial PLIF and PIV fields. The OH* spontaneous emission signal is used as the time reference signal and the phase-locked mean cycle is decomposed in 20 phases, every $18° \pm 9°$, using approximately 200 fields for each phase. Results are presented in Fig. 8.

Results clearly show the strong impact of the PVC on the droplet behavior, where up to 20 $\mathrm{m\,s^{-1}}$ in the velocity fluctuations are encountered, corresponding to a fluctuation of 20% around the mean velocity value. As expected, velocity fluctuations are almost in phase with the Mie intensity ones. More interestingly, fluctuations of the OH* emissions are out of phase with the Mie intensity and velocity ones, and one would like to relate this behavior to the evaporation time of droplets. Further investigations are being carried out on this last point.

To conclude, using the phase-averaged method applied to PLIF and HSPIV in transverse planes going from 5 to 40 mm of the injection's exit (results are not presented in the present study), it is possible to obtain a three-dimensional reconstruction of the dynamical behavior of both flame and droplets, thus enhancing the physical comprehension of their interaction. The reconstruction at a given phase value is presented in Fig. 9. An interesting feature is the spatial differences existing between spray (Mie) and heat release (OH) fluctuations.

5. Conclusion

A laboratory-scale staged multi-injection combustor is described in the present article, in the framework of LPP combustion. Using a staging procedure between the primary pilot stage and the secondary multipoint one, droplet and velocity field distributions can be varied in the spray that is formed at the entrance of the combustion chamber, influencing the dynamics of the flame. Three operating conditions are analyzed while power is kept constant. The flame structure and the spray behavior are characterized using HSPIV and PLIF in the axial direction. Results show that the flame stabilization is strongly influenced by the fuel distribution. Furthermore, it was found that for the same staging value, the flame can be stabilized either in the pilot region or in the combustion chamber, leading to a more or less strong thermo-acoustic activity. Both cases reveal the presence of a PVC in the flow that is strongly affected by the acoustic perturbation. Indeed, for the OP_{60}^{-} case where the acoustic amplitude is lower, results indicate a behavior of droplets and flame mainly driven by a

strong PVC. For the OP_{60}^{+} case, high acoustic perturbations occur leading to a very fluctuating PVC and the flow is mainly driven by the acoustic motion. The interaction between PVC and the acoustic field is still not fully understood but it seems that the burner stability and behavior are strongly influenced by the acoustic perturbation level.

Acknowledgements

This work is supported by Pôle ASTECH and funded by Conseil Régional d'Ile-de-France (CRIF), in the framework of the INCA initiative (TOSCA project). The authors would like to thank the technical staff at the EM2C laboratory for their help in designing and mounting the experimental setup.

References

[1] S. Correa, Power generation and aeropropulsion gas turbines: from combustion science to combustion technology, Proceedings of the Combustion Institute 27 (1998) 1793–1807.
[2] R. Tacina, Low NOx potential of gas turbine engines, in: AIAA Aerospace Sciences Meeting and Exhibit, 1990.
[3] A. Lefebvre, The role of fuel preparation in low-emission combustion, Journal of Engineering for Gas Turbines and Power 117 (1995) 617–654.
[4] M. Moore, NOx emission control in gas turbines for combined cycles cycle gas turbine plant, Journal of Power and Energy 211 (1997) 43–52.
[5] T. Lieuwen, V. Yang, Combustion Instabilities in Gas Turbine Engines: Operational Experience, Fundamental Mechanisms, and Modeling, Progress in Astronautics and Aeronautics, vol. 210, American Institute of Aeronautics and Astronautics, 2006.
[6] S. Candel, Combustion dynamics and control progress and challenges, Proceedings of the Combustion Institute 29 (2002) 1–28.
[7] A. Nauert, P. Petersson, M. Linne, A. Dreizler, Experimental analysis of flashback in lean premixed swirling flames: conditions close to flashback, Experiments in Fluids 43 (2007) 89–100.
[8] A. Lefebvre, Gas Turbine Combustion, 2nd edition, Taylor & Francis, 1999.
[9] S. Ducruix, T. Schuller, D. Durox, S. Candel, Combustion dynamics and instabilities: elementary coupling and driving mechanisms, Journal of Propulsion and Power 19 (2003) 722–734.
[10] Y. Neumeier, B.T. Zinn, Experimental demonstration of active control of combustion instabilities using real-time modes observation and secondary fuel injection, Proceedings of the Combustion Institute 26 (1996) 2811–2818.
[11] J. Lee, K. Kim, D. Santavicca, Effect of injection location on the effectiveness of an active control system using secondary fuel injection, Proceedings of the Combustion Institute 28 (2000) 739–746.
[12] D. Bernier, S. Ducruix, F. Lacas, S. Candel, N. Robart, T. Poinsot, Transfer function measurements in a model combustor: application to adaptive instability control, Combustion Science and Technology 175 (2003) 993–1013.
[13] S. Tachibana, L. Zimmer, Y. Kurosawa, K. Suzuki, Active control of combustion oscillations in a lean premixed combustor by secondary fuel injection coupling with chemiluminescence imaging technique, Proceedings of the Combustion Institute 31 (2007) 3225–3233.
[14] S. Barbosa, M. De la Cruz Garcia, S. Ducruix, B. Labegorre, F. Lacas, Control of combustion instabilities by local injection of hydrogen, Proceedings of the Combustion Institute 31 (2007) 3207–3214.
[15] F. Batarseh, M. Gnirß, I. Roisman, C. Tropea, Fluctuations of a spray generated by an airblast atomizer, Experiments in Fluids 46 (2009) 1081–1091.
[16] S. Barbosa, P. Scouflaire, S. Ducruix, Time resolved flowfield, flame structure and acoustic characterization of a staged multi-injection burner, Proceedings of the Combustion Institute 32 (2009) 2965–2972.
[17] S. Barbosa, Etude expérimentale d'un injecteur multipoint étagé, Ph.D. thesis, Ecole Centrale Paris, 2008.
[18] D. Galley, S. Ducruix, F. Lacas, D. Veynante, Mixing and stabilization study of a partially premixed swirling flame using laser induced fluorescence, Combustion and Flame 158 (2011) 155–171.
[19] B. Higgins, M. McQuay, F. Lacas, J. Rolon, N. Darabiha, S. Candel, Systematic measurements of OH chemiluminescence for fuel-lean, high-pressure, premixed laminar flame, Fuel 80 (2001) 67–74.
[20] M. Lauer, T. Sattelmayer, On the adequacy of chemiluminescence as a measure for heat release in turbulent flames with mixture gradients, Journal of Engineering for Gas Turbines and Power 132 (2010) 061502.
[21] M. Lauer, M. Zellhuber, T. Sattelmayer, C.J. Aul, Determination of the heat release distribution in turbulent flames by a model based correction of OH* chemiluminescence, Journal of Engineering for Gas Turbines and Power 133 (2011) 121501.
[22] T. Providakis, P. Scouflaire, L. Zimmer, S. Ducruix, Time-resolved PIV measurements applied to a non-reactive dodecane–air mixture in a two-staged multi-injection burner, in: 15th International Symposium on Applications of Laser Techniques to Fluid Mechanics, 2010.
[23] T. Providakis, L. Zimmer, P. Scouflaire, S. Ducruix, Effect of fuel distribution on spray dynamics in a two-stage multi-injection burner, in: Proceedings of ASME Turbo Expo (GT2011-46519), Vancouver, Canada, 2011.
[24] M. Rachner, J. Becker, C. Hassa, T. Doerr, Modelling of the atomization of a plain liquid fuel jet in crossflow at gas turbine conditions, Aerospace Science and Technology 6 (2002) 495–506.
[25] I. Boxx, M. Stöhr, C. Carter, W. Meier, Temporally resolved planar measurements of transient phenomena in a partially pre-mixed swirl flame in a gas turbine model combustor, Combustion and Flame 157 (2010) 1510–1525.
[26] A.M. Steinberg, I. Boxx, M. Stöhr, C.D. Carter, W. Meier, Flow–flame interactions causing acoustically coupled heat release fluctuations in a thermo-acoustically unstable gas turbine model combustor, Combustion and Flame 157 (2010) 2250–2266.
[27] J.P. Moeck, J.-F. Bourgouin, D. Durox, T. Schuller, S. Candel, Nonlinear interaction between a precessing vortex core and acoustic oscillations in a turbulent swirling flame, Combustion and Flame 159 (2012) 2650–2668.
[28] P. Iudiciani, C. Duwig, Large eddy simulation of the sensitivity of vortex breakdown and flame stabilisation to axial forcing, Flow, Turbulence and Combustion 86 (2011) 639–666.